Stress and dislocations in thin metal layers

Nicola, Lucia

Chapter 7

Freestanding thin films under tensile loading: a comparison with experiments

While previous chapters were concerned with structures on top of large substrates, this chapter deals with free-standing thin films. The tensile deformation is now applied directly to the film rather than via the substrate. Vlassak and co-workers at Harvard University employ a bulge test machine that offers the possibility of performing a tensile test under plane strain conditions [1]. The latter provides an excellent opportunity for our two dimensional plane strain discrete dislocation plasticity simulations to be confronted with experiments.

Xiang et al. [1] find a thickness dependent response of passivated films that is qualitatively similar to the one we found for polycrystalline films on a substrate [2] (see chapter 4). By simulating free-standing thin films under tension, we intend to reproduce the experimental curves, by fitting some of the unknown parameters we have used in previous simulations, such as dislocation source density and strength. The dependence of hardening on the presence of a passivation layer is also analyzed.

7.1 Main experimental results obtained by Xiang et al.

To start with, freestanding Cu films have been prepared with various thickness ($h = 0.98$, 1.9 and 4.2 μm) but constant microstructure [1]. This is achieved by vacuum annealing 5.2 μm thick Cu membranes at high temperature to stabilize the grain size and by subsequently thinning them to the required thickness by mechanical polishing. For each thickness three specimens are prepared: (i) with no passivation, (ii) with one side passivated by 20 nm Ti, (iii) with both sides passivated.

After preparation the specimens are analyzed to check if the microstructure is effectively independent of the specimen thickness. As expected, both grain size

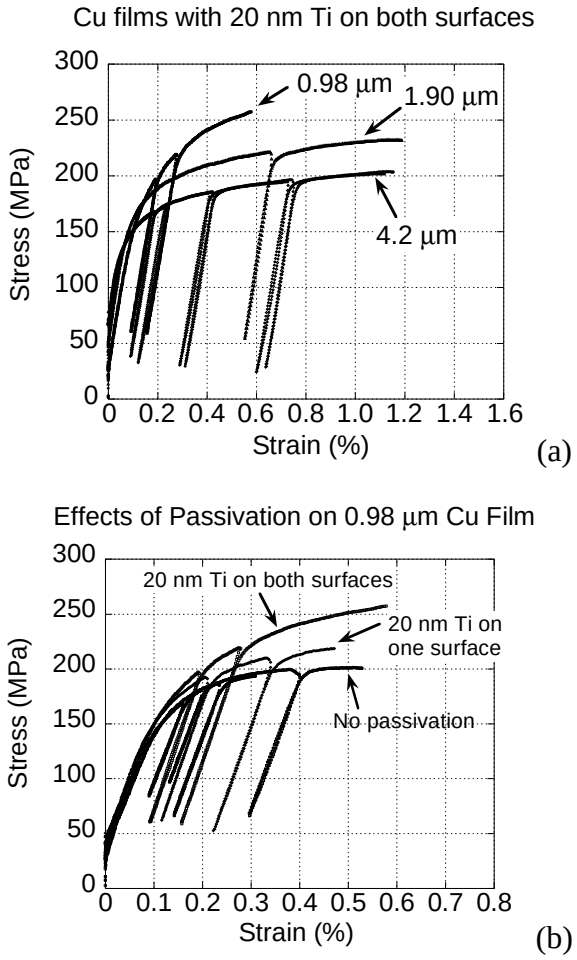

Figure 7.1 (a) Size effect in passivated freestanding films. (b) Influence of the presence of passivation layers (from [1]).

and crystallographic texture are found to be roughly the same in the different films. The mean grain size ranges from $d = 2.4\mu$m in the thinnest film to $d = 2.9\mu$m in the thickest. TEM observations show the presence of extensive twinning in all specimens and absence of dislocations.

The results of the experiments are summarized in Fig. 7.1. Figure 7.1a shows stress-strain curves as a function of film thickness for the films with both surfaces passivated; the size effect is evident. Figure 7.1b shows the effect of the coating

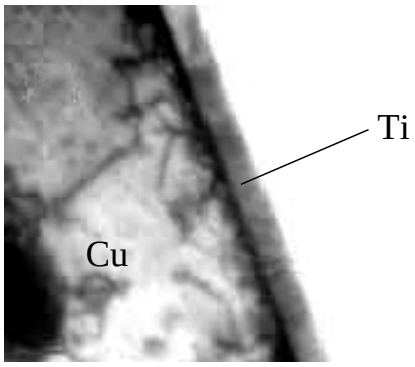

Figure 7.2 Dislocation pile-ups close to the Cu–Ti interface after deformation (from [1]).

on hardening for the thinnest films. Hardening of the thinnest film increases with the number of passivated surfaces. For the thicker films the effect is much less pronounced [1].

After deformation (up to 0.35% residual strain) the specimens are again observed at the TEM. It is observed that many dislocations have piled up close to the film–coating interface (see Fig. 7.2). The thickness of the layer with high dislocation density is only around 50 nm.

7.2 Two-dimensional model for a freestanding film

The free-standing film is modeled as an infinite array of rectangular grains of height h and width d. The film is periodic in x_1-direction with periodicity w. The unit cell is taken to contain eight grains, each of them characterized by a certain crystal orientation, given by the orientation of three sets of slip systems. The angle between the three sets of parallel slip planes in a grain is 60°. The orientation of the grain is identified by the angle ϕ at which the three sets of planes are inclined with respect to the film–coating interface. The angle ϕ for each grain is chosen at random. Two passivation layers of thickness p are coating the film.

Tension is imposed by a uniform displacement difference between cells that linearly increases in time. While the passivation layers respond elastically, plastic relaxation occurs in the film by glide of edge dislocations on the slip planes in the grains. The grain boundaries as well as the film–coating interfaces are taken to be

flat and perfectly impenetrable for dislocations. Since the elastic constants of the film (Cu) and the coating (Ti) are very similar, we take them to be the same in the simulations. Elastic anisotropy is ignored.

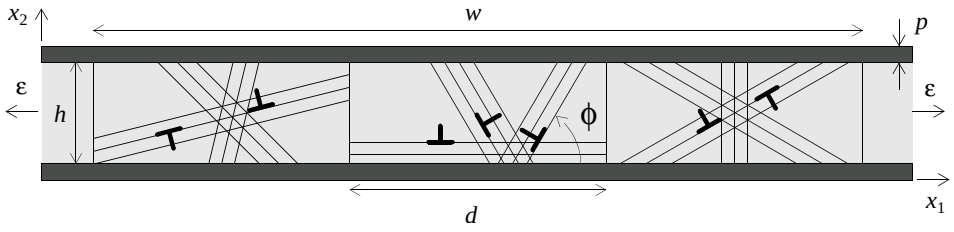

Figure 7.3 Two-dimensional model of a freestanding passivated thin film under tensile loading.

7.3 Method of analysis

The solution of the problem is obtained using the Van der Giessen-Needleman approach presented in [3]. The methodology is based on the solution of an elastic boundary value problem for the unit cell, with boundary conditions changing while the dislocation structure evolves. The complete solution is obtained, at each incremental step of the simulation, by adding the singular elastic fields of the discrete dislocations to the solution of the boundary value problem.

The governing equations for the boundary value problem, which is solved here by finite elements, are

- the equilibrium condition

$$\sigma_{ij,j} = 0 \tag{7.1}$$

- the compatibility equation

$$\varepsilon_{ij} = \frac{1}{2}(u_{i,j} + u_{j,i}) \tag{7.2}$$

- the constitutive equation

$$\varepsilon_{ij} = \frac{1+\nu}{E}\left(\sigma_{ij} - \frac{\nu}{1+\nu}\delta_{ij}\sigma_{kk}\right). \tag{7.3}$$

Tensile loading is prescribed by enforcing

$$u_i(0,x_2) = u_i(w,x_2) + U\delta_{i1} \tag{7.4}$$

at the periodic boundaries of the unit cell (δ_{ij} is the Kronecker delta). The cell-to-cell displacement $U = U_0 + \int \dot{U} dt$ increases linearly with time and determines the overall tensile strain as $\varepsilon = U/w$. At the top and bottom surfaces traction-free conditions are prescribed,

$$\sigma_{12}(x_1,0) = \sigma_{22}(x_1,0) = 0, \qquad \sigma_{12}(x_1,h+2p) = \sigma_{22}(x_1,h+2p) = 0\,, \tag{7.5}$$

where p is the thickness of the passivation layer.

Additional constitutive equations are introduced to determine the evolution of the dislocation ensemble, governed by the resolved shear stress on the slip planes. The rules control nucleation of the dislocation dipoles from point sources, dislocation glide, annihilation and pinning of dislocations at point obstacles. The simulations start from a dislocation free state and with sources randomly distributed on the slip planes. Each source is characterized by a critical nucleation strength τ_{nuc}, chosen out of a Gaussian distribution of strengths. A source becomes active when the resolved shear stress on it is larger than τ_{nuc} for a time span t_{nuc}. When this happens, a dislocation couple is generated: two dislocations of opposite sign are introduced on the slip plane at a distance L_{nuc}. This distance is such that the attractive stress field that the dislocations exert on each other is equilibrated by the resolved shear stress at nucleation (τ_{nuc}):

$$L_{\text{nuc}} = \frac{\mu}{2\pi(1-\nu)} \frac{b}{\tau_{\text{nuc}}}\,. \tag{7.6}$$

After nucleation, dislocations glide, driven by the Peach-Koehler force acting on them. For any dislocation I the Peach-Koehler force is computed as

$$f^{(I)} = n_i^{(I)} \left(\hat{\sigma}_{ij} + \sum_{J \neq I} \sigma_{ij}^{(J)} \right) b_j^{(I)}\,, \tag{7.7}$$

with $n_i^{(I)}$ denoting the normal to the slip plane of dislocation I and $b_j^{(I)}$ its Burgers vector. Here, $\tilde{\sigma}_{ij}^{(J)}$ is the long-range, singular stress field of dislocation J and $\hat{\sigma}_{ij}$ is the image stress field computed by finite elements. Dislocation climb is not accounted for. In case two opposite signed dislocations are closer to each other than the critical distance L_{ann} they are supposed to annihilate and are removed

from the calculation. Impenetrable point obstacles are present at grain boundaries and at the film–coating interface. When a dislocation arrives at an obstacle, it gets pinned there.

The conditions (7.4) and (7.5) prescribed at the boundaries of the unit cell are not sufficient to find a solution for our problem. It is necessary to apply an additional constraint in order to prevent rigid body motion of the structure. This is done by fixing a single node of the mesh; for instance by prescribing

$$u_i(0,0) = 0. \tag{7.8}$$

Due to the periodic nature of the problem, this condition corresponds to imposing $u_i(0,nw) = 0$, for $n = 0,1,2....$ This leads to a correct uniform solution as long as the response is elastic. As soon as dislocations are nucleated, the uniformity of the field brakes down and because of the constraint imposed by the fixed nodes, the film starts to bend. With increasing plastic deformation, a wave of period w forms in the film. This is directly seen in the deformed mesh shown in Fig. 7.4 but can also be recognized in the stress distribution in Fig. 7.5.

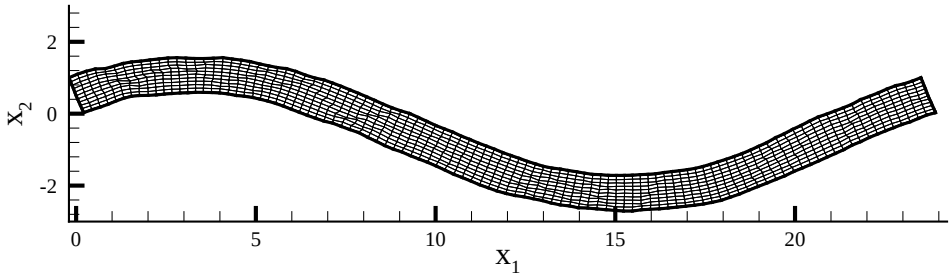

Figure 7.4 Deformed mesh for a passivated film with boundary conditions (7.4), (7.5) and (7.8) at 0.5% imposed strain. The displacements are magnified by a factor 20 for visibility.

This pronounced bending is quite unrealistic. Real films, extended in the out-of-plane direction, will not exhibit this behavior since the columnar grains are constrained by adjacent grains located in front of and behind the plane of view; this is illustrated schematically in Fig. 7.6. These grain-grain interactions are likely to constrain the film deflection in the x_2 direction. In order to mimic this with our two dimensional model, we consider it more appropriate to impose an additional constraint, namely zero vertical displacements along the centerline,

$$u_2(x_1, h/2) = 0. \tag{7.9}$$

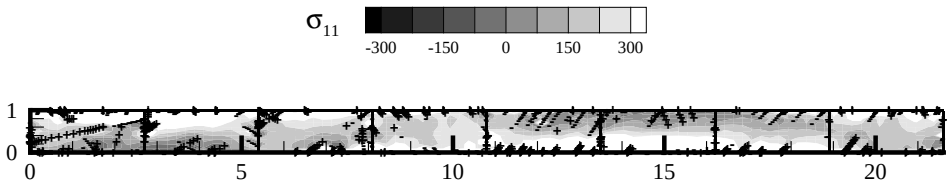

Figure 7.5 Stress and dislocation distribution at 0.5 % applied strain for the passivated film in Fig. 7.4.

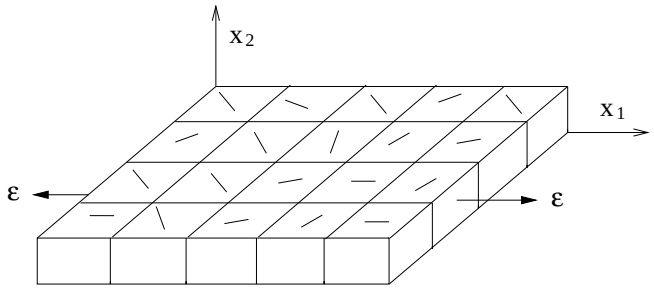

Figure 7.6 Schematic representation of a freestanding film in three dimensions: surrounding grains have different crystal orientations.

To test to which extent the condition (7.9) controls a mesh dependent response, simulations are carried out for passivated films of grain size $d = 2.7\mu$m using condition (7.9), or a weaker form of it,

$$u_2(nd, h/2) = 0, \qquad n = 0, 1, 2... \tag{7.10}$$

where only the grain boundaries are constrained. Curves for the average tensile stress,

$$\langle \sigma_{11} \rangle = \int_0^w \int_0^{h+p} \hat{\sigma}_{ij} + \sum_J \sigma_{ij}^{(J)} dx_1 dx_2$$

versus strain are shown in Fig. 7.7. The third curve is the response of the simulation shown in Fig. 7.4 and 7.5, based on (7.8) without any prescription at the middle nodes. Considering that the results for boundary condition (7.9) and (7.10) do not differ much, we choose to continue the analysis by using condition (7.9).

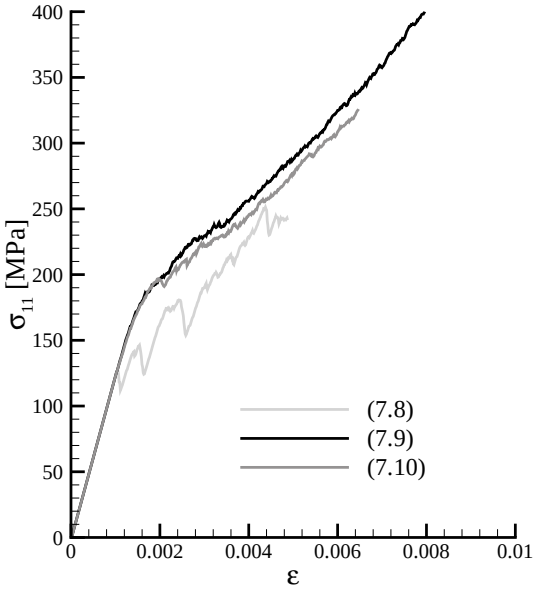

Figure 7.7 Stress–strain curves for freestanding passivated films with different b.c.

7.4 Numerical results

7.4.1 Effect of film thickness on the plastic response of coated films

The simulations are performed for films of the same thickness as tested by Xiang et al. [1], $h = 1$, 1.9 and 4.2 μm. The choice of a grain size d suitable for the comparison is less straightforward: the average grain size reported by [1] is $d = 2.7\mu$m, but the presence of many twins suggests the necessity of considering a higher density of grain boundaries. Since twinning is accompanied by crystal rotation, we will model twins in the same way we model grains. Hence, for the simulations we take $d = 1.5\mu$m, the average grain size measured in the specimens when twins are included.

The films are passivated on both sides by elastic coatings of thickness $p =$ 20nm. The films are subjected to a displacement rate of $\dot{U} = 3 \times 10^4 \mu\text{m/s}$.

The calculations start with stress free and dislocation free films. Dislocation sources are evenly distributed among the grains, randomly positioned on the slip planes. Parallel slip planes are spaced by 200 Burgers vectors. The density of dislocation sources, their average critical strength and standard deviation are un-

known values and therefore are treated here as the parameters that can be fitted to the experimental results. The average stress-strain curves are shown in Fig. 7.8. A reasonable fit to the experimental results for all thicknesses (see Fig. 7.1a) is obtained by using a source density of $15/\mu m^2$ with a mean strength of 100 MPa and a standard deviation of 20 MPa. The source density mainly determines the hardening rate (here hardening is approximately linear) and the source strength determines the flow strength. Results are strongly dependent on these two values. On the contrary, dependence on the standard deviation of the source strength distribution is found to be very weak. While in single crystal simulations it is essential that this value is different from zero to prevent simultaneous nucleation of sources on slip planes with the same Schmid factor (see chapter 2), the variety of slip plane orientations accounted for in polycrystals is already sufficient to ensure that the nucleation events occur at different moments.

Figure 4.7 shows stress state and dislocation distribution in the films at 0.35% residual strain. Grain boundaries are characterized by a high dislocation density. Hard boundary layers are present at the film–coating interfaces.

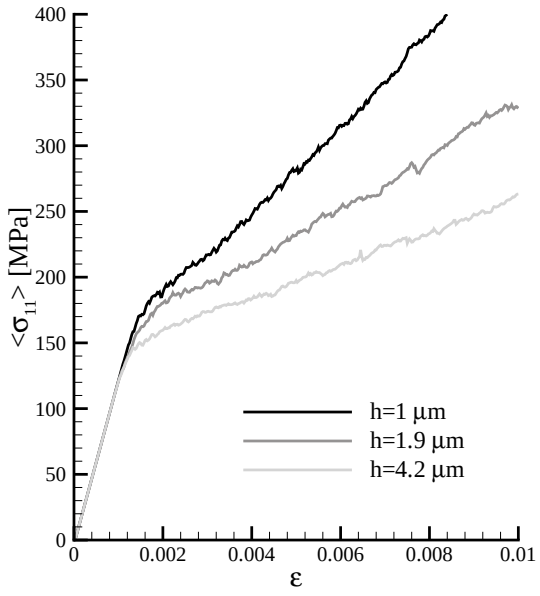

Figure 7.8 Size effect: simulated stress-strain curves for free-standing films with double-sided passivation.

7.4.2 Effect of passivation layer

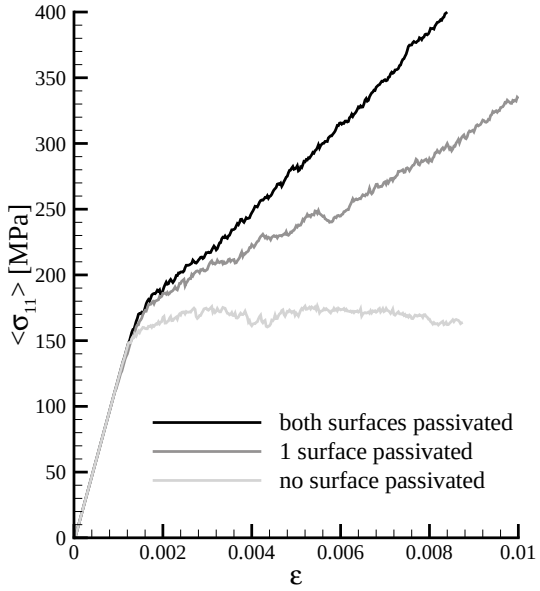

Figure 7.9 Effect of the presence of passivation layer(s) on hardening.

Figure 7.9 shows the average stress $\langle\sigma_{11}\rangle$ versus strain curves for the thinnest film without passivation, and with one or both sides passivated. In agreement with the experiments (see Fig. 7.1b), the simulations show that hardening increases with the number of passivation layers. But, while in experiments hardening occurs even for bare films, the simulated bare film does not harden. The reason for this is that two-dimensional discrete dislocation simulations are able to capture hardening only if sufficiently many dislocations remain inside the film, pinned either at obstacles or boundaries. The reason is that the presence of discrete dislocations influences the stress state at the sources and therefore the nucleation activity. In the case of a bare film, coatings are not present to stop dislocations from leaving the film surfaces and the density of grain boundaries is too low to stop a significant number of dislocations. A few sources on slip planes that do not cross grain boundaries carry out most of the relaxation by continuously nucleating dislocations that subsequently glide out of the film. Contrary to simulations of passivated films, simulations of bare films are strongly dependent on the standard deviation of dislocation strength: the weakest sources are responsible for the

whole relaxation and the strongest never get activated.

7.5 Conclusions

In this chapter a comparison between experimental results and results of discrete dislocation plasticity simulations of free-standing films under tension has been presented. Experimental results and discrete dislocation simulation results are in qualitative good agreement: they both capture the thickness dependent hardening of passivated films and a dependence of hardening on the presence of passivation layers. The best fit has been obtained by using a source density of $15/\mu m^2$ with a mean strength of 100 MPa and a standard deviation of 20 MPa.

References

[1] Y. Xiang, J.J. Vlassak, M.T. Perez-Prado, Mat. Res. Soc. Symp. Proc. **795** (2003).

[2] L. Nicola, E. Van der Giessen, A. Needleman, J. Mater. Res., in press.

[3] E. Van der Giessen, A. Needleman, Simul. Mater. Sci. Eng. **3** (1995) 689.